



# Structural health monitoring of beam model based on swarm intelligence-based algorithms and neural networks employing FRF

Fatima Achouri<sup>1</sup> · Abdelwahhab Khatir<sup>2</sup> · Zakaria Smahi<sup>3</sup> · Roberto Capozucca<sup>2</sup> · Abdelmoumin Ouled Brahim<sup>2</sup>

Received: 11 January 2023 / Accepted: 5 October 2023 / Published online: 7 November 2023  
© The Author(s) 2023

## Abstract

In recent decades, swarm optimization methods have been employed to address various optimization problems in structural health monitoring (SHM). One of the widely recognized swarm-based algorithms, particle swarm optimization (PSO), has gained significant popularity and found extensive applications across diverse fields. However, it presents some limitations, such as the low convergence rate in the iterative process. The butterfly optimization algorithm (BOA) is a recently developed algorithm that has demonstrated its performance in solving a variety of optimization problems. In this research, a novel hybrid swarm optimization algorithm is introduced, integrating PSO and BOA, with the aim of enhancing its effectiveness. To overcome the limitations of the traditional Artificial Neural Network (ANN) technique and enhance its training performance, this new hybrid algorithm is integrated with ANN. The study offers valuable insights into the creation of a predictive model, known as PSO-BOA-ANN, for detecting structural damage. Input parameters for the model include natural frequencies, while the output parameter is the severity of the damage. To test the efficiency of the proposed technique, data were collected from a finite element model using a simulation tool, and from frequency response function (FRF) after experimental modal analysis for single and double cracked aluminum beams considering different crack depths. A comparative analysis was conducted between the results obtained from PSO, BOA, GA, and their respective combinations with ANN. The findings indicate that the novel PSO-BOA-ANN approach outperforms the other approaches in terms of accuracy when it comes to damage prediction.

**Keywords** Structural health monitoring · Swarm optimization algorithms · Artificial neural network · Modal analysis · Finite element analysis

## 1 Introduction

Structure health monitoring (SHM) is a multidisciplinary domain that involves measuring structural loads and responses automatically and diagnosing structural health

using a variety of instruments and sensors. Scientists and administrative authorities have recognized the importance of long-term SHM systems for civil infrastructures over a significant period. These systems play a crucial role in ensuring structural safety and detecting potential issues in a timely manner, thereby preventing costly and potentially catastrophic consequences. There are several components that make up SHM systems, including sensors, data acquisition devices, transmission systems, databases, data analysis programs, alarm devices, software, and operating systems [1]. Mechanical, aerospace, and civil engineering are among the fields that have adopted SHM systems [2–7].

The use of evolutionary algorithms to solve linear and nonlinear problems in engineering has recently been demonstrated using particle swarm optimization and genetic algorithms [8–11]. Moreover, it has been used for damages prediction in different civil structures like bridge piers [12, 13], Tunnels [14], and dike [15]. There have been a

---

Technical Editor: Samuel da Silva.

✉ Abdelwahhab Khatir  
a.khatir@pm.univpm.it

<sup>1</sup> Department of Civil Engineering, Mustapha Stambouli University of Mascara, 305, Mamounia Road Mascara, Algeria

<sup>2</sup> Structural Section DICEA, Polytechnic University of Marche, Brecci Bianche 10, 60131 Ancona, Italy

<sup>3</sup> Department of Engineering Physics, University of Sciences and Technologies Mohamed Boudiaf of Oran (USTO-MB), 1505, EL MNAOUER, 31000 Oran, Algeria

number of other optimization algorithms used to solve SHM problems, including Cuckoo Search algorithms (CS) [16, 17], Firefly algorithms (FA) [18], Artificial Bee Colonies (ABC) [19], Ant Colony Optimizations (ACO) [20], BAT Algorithm [21, 22], and Harmony Search algorithms (HS) [23]. In their study, Na et al. [24] employed a genetic algorithm (GA) to identify and assess damages in a large-scale building. It was still possible to determine damage locations and severity, even though measured data for the considered structures were incomplete. Yildiz [25] utilized the cuckoo search (CS) algorithm to present optimization problems in the manufacturing domain. Specifically, CS was applied to optimize milling processes, and its performance was compared with other algorithms such as PSO, Ant Colony (AC) algorithm, and immune algorithm. A comparison of CS and the aforementioned algorithms revealed CS to be superior. Using static deflections, mode shapes, and natural frequencies as objective functions, Jung et al. [26] utilized a hybrid GA to perform updates on a small-scale bridge.

Artificial intelligence techniques, such as artificial neural networks (ANN), have proven to be highly effective in resolving engineering SHM issues. Reduced mode shapes and computational tools were used by Gomes et al. [27] to apply an improved technique for GA and ANN-based delamination detection of CFRP laminated composite plates. Kellouch et al. [28] utilized an artificial neural network (ANN) to estimate the lifespan of fly ash concrete. They developed a prediction model based on carbonation depth to accurately assess the concrete's durability. According to tests done to verify the created model, ANN is a reliable technique for forecasting the carbonation depth of fly ash concrete. An ANN model was employed to characterize the tensile behavior of hybrid fiber reinforced concrete (HFRC) beyond the stress–strain curve [29]. This ANN model provided a comprehensive description of the concrete's response to tensile stress. The results indicate that the ANN model outperforms the equation-based model in accurately predicting the tensile stress–strain curve, tensile strength, and strain associated with the tensile strength of HFRC. To estimate the fracture energy of polymer nanocomposites, Hamdia et al. [30] integrated ANN with an adaptive neuro-fuzzy inference system (ANFIS). The creation, training, and testing of ANN and ANFIS models utilized a collection of 115 experimental datasets sourced from existing literature. The results obtained using the latter method were significantly superior, as evidenced by lower values of root mean square error and mean absolute percentage error. For the purpose of predicting beam fractures, Khatir et al. [31] proposed a vibration-based method combining ANN and Butterfly Optimization Algorithm (BOA) for crack depth prediction in different locations in a steel beams. The crack depth is the output, and natural frequencies are the input parameters. Its precision demonstrates that BOA-ANN produces accurate results. They have proposed also new approaches such PSO-Yuki and Radial Bases Function to deal

with crack identification in carbon fiber reinforced polymer beam models [32] and RC beams [33]. According to an algorithm provided by Dunant et al. [34], the sets of interacting degrees of freedom are generated dynamically as the material's state changes. Consequently, a modified Newton approach was used to solve a non-local damage model. Jierula et al. [35] introduced a deep learning methodology aimed at identifying damaged areas within pile foundations based on acoustic emission data. As a result, it is possible to assess the concrete structures' degradation progression using the trained classification learner.

For the past few decades, the investigation of dynamic responses has emerged as a highly active research domain within the field of structural damage detection. The primary identification methods rely on changes in natural frequencies [36], modal shapes [37], and frequency response function (FRF) [38–41]. In order to identify damage to a beam, Salehi [42] exploited both real and imagined portions of FRF forms. The identification of damage is accomplished through the Gapped Smoothing Method (GSM), which detects modifications in the shapes of FRFs resulting from the damage. FRFs were used by Golafshani et al. [43] to identify damage to shear buildings. A minimum rank perturbation theory was used in order to locate the damage position.

Using numerical and experimental vibration analysis as training data sources, this paper aims to address the limitations of existing predictive models for structural damage by introducing a novel hybrid approach called PSO-BOA-ANN. The motivation behind this research lies in the need for accurate and efficient crack depth prediction in aluminum beam models. The main goals and objectives of this study are to enhance the accuracy and convergence speed of the predictive model by integrating PSO with the recently developed BOA and to assess the performance of the improved model through a comprehensive comparison with other intelligence-based models. The novelty of this research lies in the integration of PSO and BOA to optimize the parameters of an ANN and improve its training performance. By exploring the potential of the PSO-BOA-ANN model in accurately predicting crack depths, this study contributes to the field of structural damage detection and offers valuable insights into the development of more effective and reliable predictive models. The proposed approach has the potential to advance the current state of the art in SHM and provide valuable information for damage assessment and maintenance decision-making processes.

## 2 Particle swarm optimization and Butterfly optimization algorithm

The suggested method combines PSO and BOA to develop a hybrid algorithm that is better than BOA or PSO alone. Basic concepts of both considered optimization approaches are given in this section.

## 2.1 The basic concept of particle swarm optimization (PSO)

The PSO algorithm is grounded in emulating the movement of a group of birds as they navigate a multidimensional search space in search of food. This algorithm, as described in reference [44], relies on two fundamental attributes: position and velocity. These properties are essential in determining the optimal value. In the context of the search space, each entity is denoted as a particle, and they are initially assigned random positions and velocities to initiate the optimization process. The following is the global particle that has the best location in the ideal solution:

$$v_i^{t+1} = \omega \cdot v_i^t + c_1 \cdot \text{rand}_1 \times (p_{\text{best}} - x_i^t) + c_2 \cdot \text{rand}_2 \times (g_{\text{best}} - x_i^t) \quad (1)$$

$$x_i^{t+1} = x_i^t + v_i^{t+1} \quad (2)$$

where  $v_i^{t+1}$  and  $x_i^{t+1}$  denote the velocity of the  $i$ th particle at iteration number ( $t$ ) and ( $t+1$ ), respectively. Typically, the constants  $c_1$  and  $c_2$  are both set to 2, and  $\text{rand}_1$  and  $\text{rand}_2$  represent random numbers within the range of (0, 1). The value of  $\omega$  can be calculated as follows:

$$\omega(t) = \omega^{\text{max}} - \frac{(\omega^{\text{max}} - \omega^{\text{min}}) \cdot T_i}{T_{\text{max}}} \quad (3)$$

where  $\omega^{\text{max}} = 0.9$ ,  $\omega^{\text{min}} = 0.2$  and  $T_{\text{max}}$  denotes the maximum number of iterations.

## 2.2 The basic concept of Butterfly optimization algorithm (BOA)

A meta-heuristic method called the Butterfly Optimization Algorithm [45] replicates the feeding and mating behavior of butterflies. The BOA differs from previous meta-heuristics because every butterfly has a distinctive fragrance of its own. In accordance with the degree of physical stimulation, the fragrance is produced in the following ways:

$$f_i = cI^a \quad (4)$$

In the context provided,  $f_i$  represents the perceived fragrance magnitude,  $c$  denotes the sensory modality,  $I$  represents the stimulation intensity, and  $a$  represents the power exponent, which is dependent on the degree of fragrance absorption.

In the BOA process, the value of the sensory morphology coefficient  $c$  is determined based on the specificity of the optimization problem. As the algorithm advances through the optimal search phase, the sensory modality  $c$  can be formulated as follows:

$$c_{t+1} = c_t + \left[ \frac{0.025}{c_t \cdot T_{\text{max}}} \right] \quad (5)$$

In this context,  $T_{\text{max}}$  represents the maximum number of iterations for the algorithm, and the initial value of the parameter  $c$  is set to 0.01.

The algorithm encompasses two crucial phases: the global search phase and the local search phase. Equation (6) provides a mathematical representation of the global search motions of the butterflies.

$$x_i^{t+1} = x_i^t + (r^2 \times g_{\text{best}} - x_i^t) \times f_i \quad (6)$$

where  $x_i^t$  represents the solution vector  $x_i$  of the  $i$ th butterfly in iteration number  $t$ .  $g_{\text{best}}$  denotes the current best solution identified among all the solutions in the current iteration. The fragrance of the  $i$ th butterfly is represented by  $f_i$ , and  $r$  represents a random number within the range of [0, 1]. The formulation of the local search phase can be expressed as follows:

where  $x_i^t$  is the  $i$ th butterfly's solution vector  $x_i$  in iteration number  $t$ .  $g_{\text{best}}$  is the current best solution identified among all the solutions in the current iteration. The  $i$ th butterfly's fragrance is represented by  $f_i$ , while  $r$  is a random number in the range [0, 1]. The local search phase can be formulated as follows:

$$x_i^{t+1} = x_i^t + (r^2 \times x_i^k - x_i^t) \times f_i \quad (7)$$

In this context,  $x_j^t$  and  $x_i^k$  refer to the  $j$ th and  $k$ th butterflies randomly selected from the solution space. If  $x_j^t$  and  $x_i^k$  belong to the same iteration, the butterfly undergoes a local random walk. However, if they do not belong to the same iteration, the solution becomes more diverse due to this random movement.

In nature, butterflies conduct both global and local-scale searches for food and mates. To transition from a typical global search to an intensive local search, a switch probability  $\rho$  is defined. During each cycle, the BOA generates a random number within the range of [0, 1], which is compared to the switch probability  $\rho$ . This comparison determines whether a global or local search should be performed.

## 2.3 PSO-BOA hybrid algorithm

A new hybrid PSO-BOA is introduced in this section, which is an integration of distinct BOA and PSO and new individuals are generated differently. PSO can solve high-dimensional optimization problems, but it is limited in a number of dimensions. The advantages of the two algorithms can be combined when both algorithms are used together, rather than using both

algorithms sequentially. Therefore, there is heterogeneity in the final results between both algorithms, due to the method involved in producing them. The following is the suggested hybrid:

$$v_i^{t+1} = w \cdot v_i^t + C_1 \cdot r_1 \times (p_{\text{best}} - X_i^t) + C_2 \cdot r_2 \times (g_{\text{best}} - X_i^t) \quad (8)$$

where  $C_1$  and  $C_2$  both set to 0.5, the value of  $w$  can be calculated using Eq. (3). Additionally,  $r_1$  and  $r_2$  represent random numbers within the range of (0, 1)

$$X_i^{t+1} = X_i^t + V^{t+1} \quad (9)$$

Eqs. (6) and (7) can be used to calculate the BOA's global and local search phase. The hybrid PSO-BOA search phase can be formulated as follows:

$$X_i^{t+1} = w \cdot X_i^t + (r^2 \times g_{\text{best}} - w \cdot X_i^t) \times f_i \quad (10)$$

The hybrid PSO-BOA's local search phase can be expressed as follows:

$$X_i^{t+1} = w \cdot X_i^t + (r^2 \times X_i^k - w \cdot X_j^t) \times f_i \quad (11)$$

where  $X_i^k$  and  $X_j^t$  represent the  $j$ th and  $k$ th butterflies randomly selected from the solution space, respectively (Fig. 1).

### 3 ANN training for damage detection using PSO-BOA

In this study, the utilization of an ANN, which is a machine learning technique, is implemented. It consists of interconnected neurons that work together to process information. The classic architecture of an ANN comprises an input layer, one or more hidden layers, and an output layer. Each layer can have a varying number of neurons. These neurons establish connections with each other to facilitate information flow. The determination of the ANN's topology involved a systematic approach that took into account several factors. These factors included the complexity of the problem at hand, the available computational resources, and prior knowledge gained from similar applications. We carefully

1. Generate a random initial population of the butterflies  $X_i$  ( $i = 1, 2, \dots, n$ )
2. Set the value of the parameter.  $r_1, r_2, C_1$  and  $C_2$
3. Define sensor modality  $c$ , power exponent  $a$  and switch probability  $p$
4. **Evaluate the fitness value for each butterfly**
5. **While**  $t = 1$ : the max iterations
6.     **For** each search agent
7.         Revise the fragrance of the current search agent using Equation (4)
8.     **End for**
9.     Find the best  $f$
10.    **For** each search agent
11.         Set a random number  $r$  in [0,1]
12.         **If**  $r < p$  then
13.             Move towards best position by Equation (10)
14.         **Else**
15.             Move randomly by Equation (11)
16.         **End if**
17.    **End for**
18. Adjust the velocity based on Equation (8)
19. Determine the new fitness value for each butterflies
20.     **If**  $f_{\text{new}} < \text{best } f$
21. Update the position of best  $f$  using Equation (9)
22.     **End if**
23. **Update the value of the power exponent, represented by  $a$**
24.  $t = t + 1$
25. **End while**
26. **Return the best solution along with its corresponding fitness value**

Fig. 1 Pseudo-code of hybrid PSO-BOA

considered these aspects to design an appropriate architecture for the ANN. Figure 2 illustrates the specific ANN architecture utilized in the present research.

The number of neurons in each layer is determined based on the specific problems being analyzed and the amount of data available from numerical or experimental studies. Figure 2 shows the input layer of the proposed indicator as a natural frequencies, which is then passed to the hidden layer. To examine the acquired data from the first to the last phase, we must go through the two following formulations:

$$\bar{\phi}_j = \bar{\phi} (\sum_{i=1}^n w_{ij} f_i + b_i), \quad j=(1-m) \tag{12}$$

$$O_j^1 = \frac{1}{1+e^{-\bar{\phi}_j}} \tag{13}$$

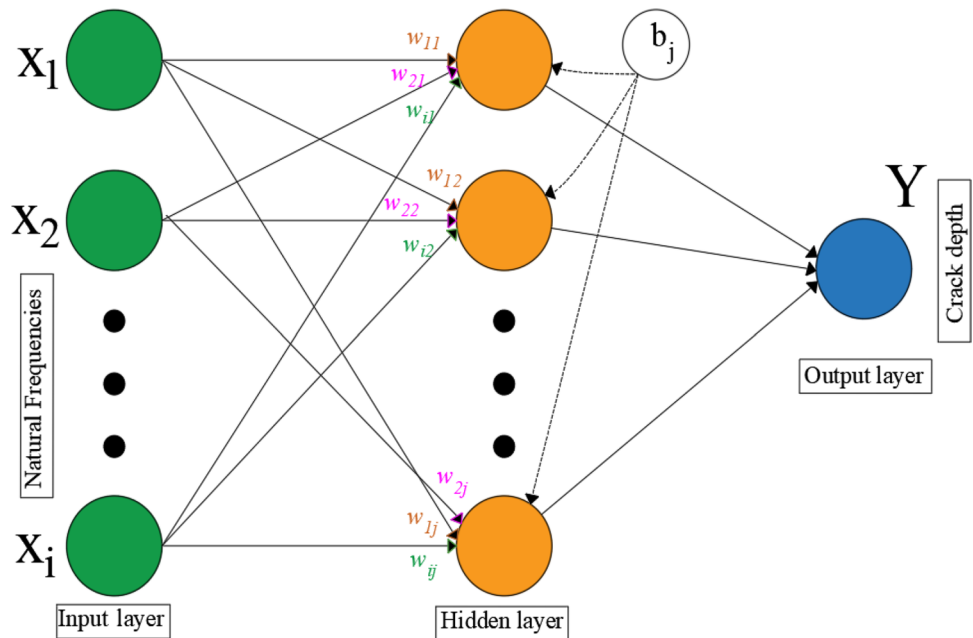
In this context,  $\bar{\phi}_j$  represents the data obtained from the  $j$ th element of the hidden layer,  $m$  determines the number of neurons utilized in the hidden layer, and  $n$  signifies the number of elements introduced into the input layer.  $f_i$  denotes the output data, while  $w$  and  $b$  refer to the weight and bias, respectively, employed for training purposes.  $w$  refers to the weight matrix that connects the neurons in different layers of ANN. It represents the strength of the connections between neurons. On the other hand,  $b$  refers to the bias vector in the ANN, which allows for shifting the activation function of each neuron. In the initial formulation (Eq. 12), the training parameters are employed to calculate the summation function. Subsequently, Eq. (13) is utilized to compute the output of the hidden layer after  $\bar{\phi}_j$  has been defined.

In this research, the PSO-BOA algorithm was utilized to optimize the weight and bias of the optimal network structure obtained from the ANN. The training process of the network involved determining the weights and biases using the Levenberg–Marquardt (LM) technique, which is based on multilayer feed-forward backpropagation. To conduct the ANN simulation, the MATLAB toolbox was employed. For solving the approximation problem, the Mean Squared Error (MSE) was adopted as the fitness function, as described in Eqs. (14) and (15). The optimal architecture of the ANN was identified by choosing the configuration that yielded the lowest MSE. Figure 3 illustrates PSO-BOA-ANN algorithm work process.

This study presents a novel contribution with the introduction of the PSO-BOA-ANN hybrid approach for structural damage detection. This approach combines the strengths of PSO and BOA to optimize the parameters of ANN for crack depth prediction. Unlike existing formulations that rely on PSO or BOA alone, our hybrid approach offers improved performance by leveraging the synergistic benefits of both algorithms. This integration enhances the accuracy and convergence speed, making it a promising solution for accurate crack depth prediction in structural health monitoring.

$$RMSE = \sqrt{\sum_{P=1}^P \sum_{i=1}^N (t_{Pi} - O_{Pi})^2 / P \times N} \tag{14}$$

Fig. 2 ANN structure for damage level determination



1. Specify the number of input parameters.
2. Initialize all parameters of the Artificial Neural Network (ANN).
3. Determine the number of hidden layers and the number of neurons ( $n=5$ ).
4. Choose the ANN training algorithm and the learning rate within the range of  $[0, 1]$ .
5. Train the neural network and extract the weights and biases.
6. Configure the parameters of the PSO-BOA algorithm as presented in Table 3.
7. Define the range of the search space for each weight and bias.
8. Use the ANN matrix weights and biases as the initial population for the PSO-BOA algorithm.
9. Define the Mean Squared Error (MSE) as the objective function to be minimized.
10. Continuously check for convergence of the error to reach a minimum.
11. Repeat the iterations until the maximum number of iterations is reached.
12. Select the global optimum solution as the final weights and biases matrix.
13. Incorporate the final weights and biases into the ANN model for predicting the crack depth.
14. End

**Fig. 3** Pseudo-code of hybrid PSO-BOA-ANN

$$\text{MSE} = 100 \times \frac{\text{RMSE}}{\sum_{P=1}^P \sum_{i=1}^N t_{pi} / P \times N} \quad (15)$$

In this context,  $N$  represents the number of output units, while  $P$  denotes the number of pattern units.

The process of determining the most suitable topology for the Artificial Neural Network (ANN) within our proposed PSO-BOA-ANN model is a pivotal aspect in achieving accurate predictions. To select the optimal topology, an extensive exploration of various configurations was undertaken, encompassing diverse numbers of hidden layers and neurons in each layer. During this phase, strategies such as early stopping and regularization were employed to curb overfitting and bolster the model's generalization capabilities. Furthermore, a meticulous cross-validation process was executed, involving the partitioning of the dataset into distinct training, validation, and testing subsets. The ANN topology that exhibited superior performance across multiple validation metrics was singled out as the best configuration. This rigorous approach ensures that the chosen ANN topology adeptly addresses the challenges posed by structural damage prediction, striking a harmonious balance between complexity and generalization.

## 4 Numerical simulation

A model of an aluminum beam is shown in Fig. 4 with geometrical and mechanical properties shown in Table 1. It has been modeled using ABAQUS 16.4 software which considers a free-free boundary condition. Three-dimensional beam modeling is completed using the eight-node C3D8R brick element. Each node has six degrees of freedom, including three rotational displacements ( $x, y, z$ ) and three translational displacements ( $u, w, v$ ). Cracks with varying depths were intentionally generated at multiple locations along the length of the beam. The undamaged (D0) beam's frequency data are presented in Table 2, obtained from both numerical simulations and experimental observations. Due to experimental constraints, the torsional modes were not considered in the analysis. The first three mode shapes, obtained from both experimental and numerical approaches, are displayed in Fig. 5. To evaluate the effectiveness of the PSO-BOA-ANN method in predicting crack depths, two damage scenarios were examined. In the first scenario (D1), a single crack was introduced in the middle of the beam, with the crack depth gradually increasing from 0.5 mm to 25 mm. In the second scenario (D2), a double crack with a separation of 350 mm was created, and the crack depth was increased from 0.5 mm

**Fig. 4** Aluminum beam model and the two examined damage cases, D1 and D2

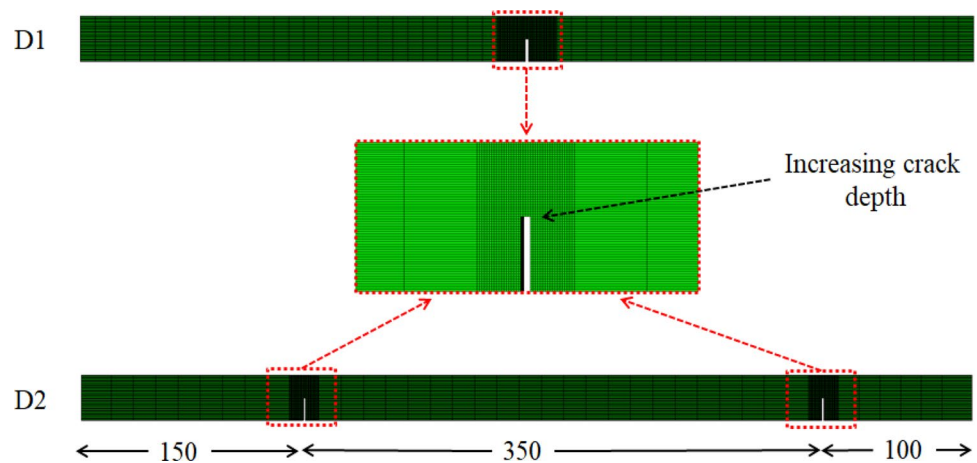


**Table 1** Geometrical and mechanical characteristics of beam model

Length $L$ (mm)	Width $W$ (mm)	Thickness $t$ (mm)	Density $\rho$ ( $\text{kg/m}^3$ )	Young modulus $E$ (GPA)
600	30	5	2710	70

**Table 2** Measured Frequencies of undamaged beam model

Modes	FEM (Hz)	Experimental (Hz)
1	400.07	385.81
2	1085.1	1097.65
3	2079.5	2102.00

to 25 mm. Consequently, a total of 50 datasets were generated for each damage scenario, resulting in a dataset of 100 instances used for training prediction models (refer to the Appendix).

The convergence criteria used for the Finite Element Model (FEM) in our study were defined based on the displacement convergence and the stress convergence. The displacement convergence criterion ensures that the solution reaches a stable state, while the stress convergence criterion ensures the accurate quantification of internal stress resultants and the corresponding stresses. These convergence criteria are essential for obtaining accurate results in FEM analysis as they indicate the convergence of the iterative solution process. The importance of convergence criteria lies in their ability to validate the quality of the solution and ensure reliable and accurate results. By

satisfying these convergence criteria, we can ensure that the analysis adequately captures the behavior of the beam under various loading conditions and accurately predicts the crack depths. Moreover, convergence criteria also play a role in controlling the computational load associated with the analysis. By achieving convergence, we optimize the computational effectiveness and reduce the computational time required for the analysis.

## 5 Results and discussion

The datasets were collected based on the analyzed results of damage cases  $D_1$  and  $D_2$  to predict the selected cracks depth of 5, 15, and 22 mm applied on beam model as shown in Fig. 4. PSO-BOA-ANN is trained considering the number of neurons is set to 5. The parameter settings for considered algorithms were determined through an iterative process of experimentation and fine-tuning. Initially, a range of values for each parameter was selected based on prior research and domain knowledge. Then, extensive experimentation was performed using different combinations of parameter values to evaluate the performance of each algorithm. The parameter settings that yielded the best results in terms of accuracy and convergence were selected for inclusion in Table 3. To study the effectiveness of PSO-BOA for ANN training, it is compared to other approaches namely PSO-ANN, BOA-ANN, and GA-ANN.

In the optimization of the proposed hybrid PSO-BOA-ANN model, the selection of appropriate parameters is crucial for achieving optimal performance. The process of determining these parameters involved a systematic and iterative approach. Initially, we conducted a comprehensive

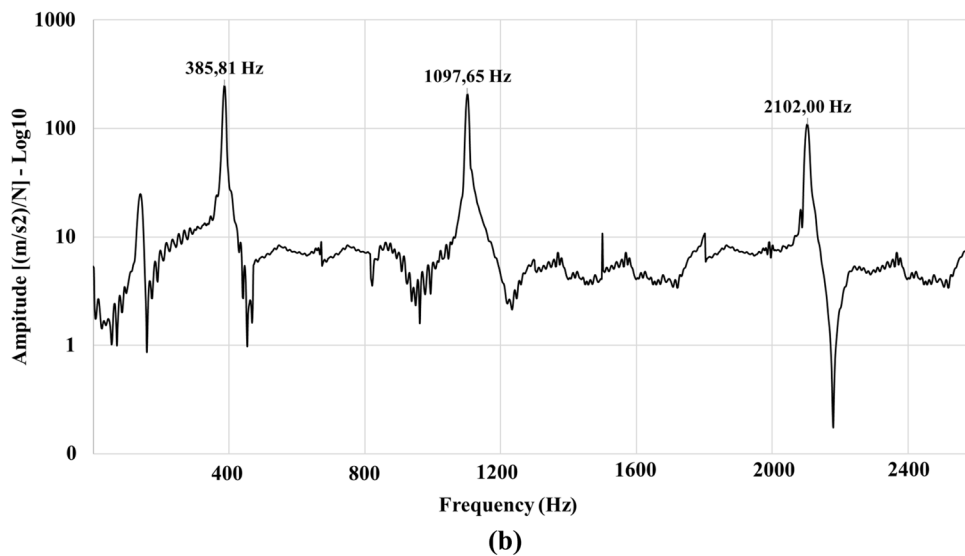
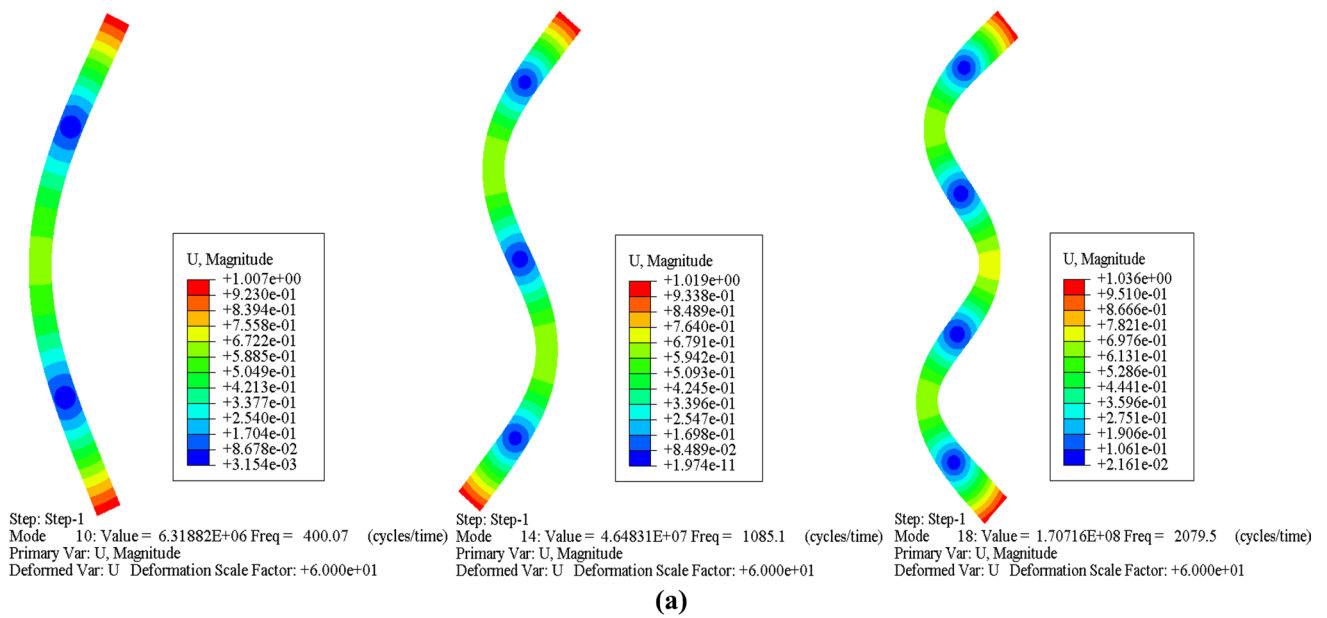


**Fig. 5** The three first mode shapes and frequencies of undamaged beam; **a** numerical, and **b** experimental frequency response function

**Table 3** Considered algorithms parameter settings

BOA	Power exponent $a$ 0.1	Switch probability $\rho$ 0.5	Sensory morphology coefficient $c(0)$ 0.01	Population size 100
PSO	Velocity $v$ $v_{\max} = 1, v_{\min} = -1$	$c_1, c_2$ coefficients $c_1 = c_2 = 2$	$\omega$ coefficient $\omega_{\max} = 0.9, \omega_{\min} = 0.2$	Population size 100
PSO-BOA	Power exponent $a$ 0.1	Switch probability $\rho$ 0.5	Sensory morphology coefficient $c(0)$ 0.01	$c_1, c_2$ coefficients $c_1 = c_2 = 0.5$
GA	Mutation 0.01	Crossover 0.8	Number of generation 200	Population size [100, 1000]



literature review to identify potential parameter ranges based on previous studies in similar domains. Subsequently, we performed a series of experiments, varying the parameters

individually and in combinations, while assessing their impact on the model's performance using validation data. This process allowed us to identify parameter configurations

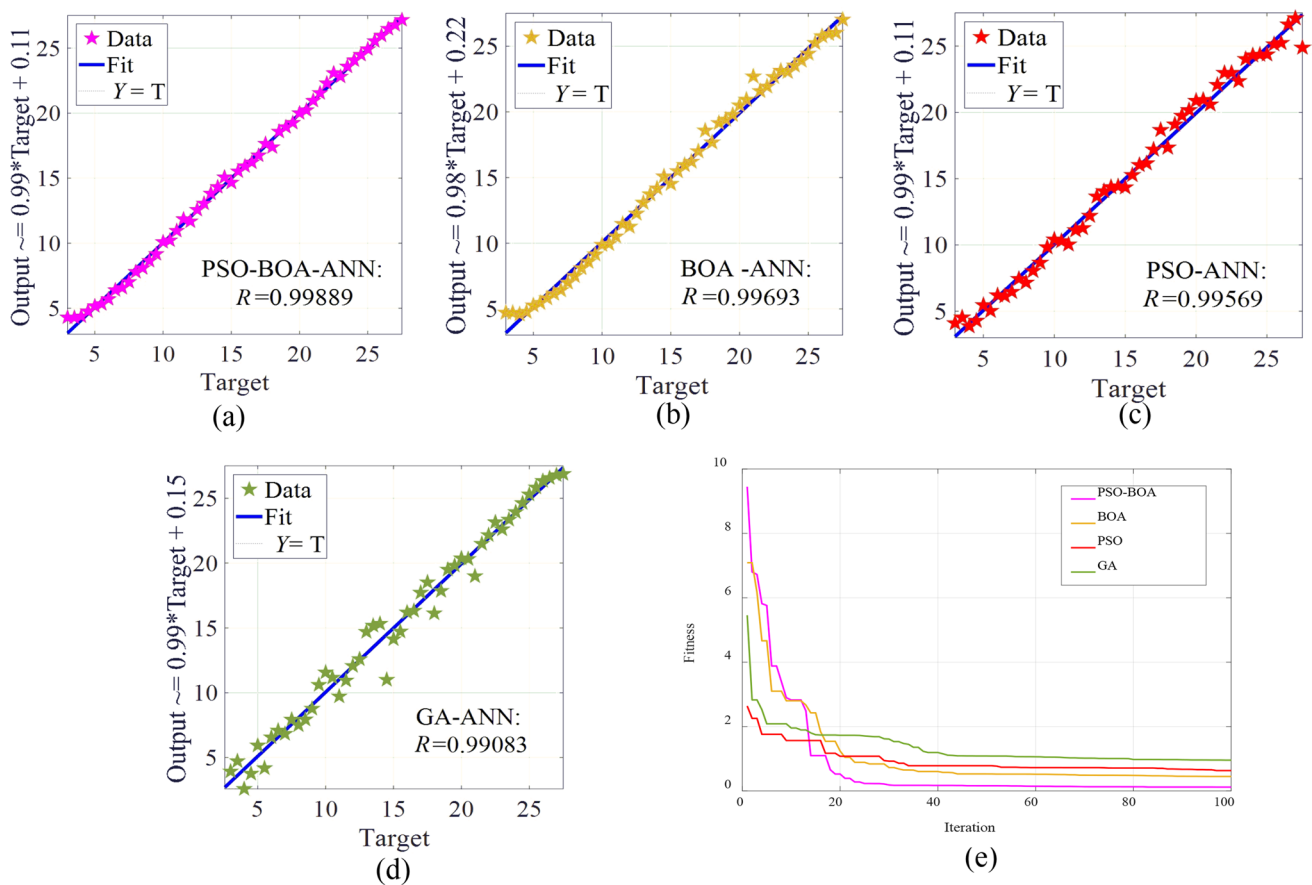


Fig. 6 Regression for damage case  $D_1$  with PSO-BOA (a), BOA (b), PSO (c), GA (d), and performance study (e)

Table 4 Crack depths predictions for damage case  $D_1$  using ANN trained by PSO-BOA, PSO, BOA, and GA

Damage case	Real crack depth (mm)	Predicted crack depth (mm)	Error in predicted results (%)	Fitness following number of iteration					
				1	25	50	75	100	
$D_1$	5	PSO-BOA	4.9880	0.240	9.46815	0.00679	0.00563	0.00034	0.00034
		BOA	5.3828	7.656	7.18666	1.10807	0.71010	0.50290	0.50290
		PSO	5.3888	7.776	2.66122	1.33205	0.90125	0.85542	0.81000
		GA	5.6101	12.202	5.53255	1.90012	1.30218	1.09250	1.00846
	15	PSO-BOA	14.9916	0.056	1.10104	0.00758	0.00011	0.00011	0.00003
		BOA	14.9312	0.459	2.20933	0.02528	0.00033	0.00026	0.00026
		PSO	15.2161	1.441	1.65485	0.11122	0.00222	0.00093	0.00093
		GA	15.6100	4.067	6.00211	1.88801	0.83213	0.03251	0.00998
	22	PSO-BOA	22.0191	0.087	0.64047	0.28256	0.03435	0.00999	0.00013
		BOA	22.2120	0.964	2.47983	0.06840	0.06840	0.01467	0.01467
		PSO	22.2999	1.363	3.65464	0.96454	0.09988	0.09988	0.03211
		GA	23.2222	5.555	7.65498	2.55444	0.91001	0.88001	0.20012

that led to improved accuracy and generalizability. Furthermore, to prevent the model from converging to local minima, we employed a range of initializations and explored a diverse set of parameter values. The final parameter values presented in Table 3 were chosen based on a trade-off between model complexity and predictive accuracy. This approach ensures that the selected parameters are robust and well-suited for the task of structural damage prediction.

### 5.1 Damage case D<sub>1</sub>

In this specific damage instance, PSO-BOA-ANN has employed to forecast single crack depths at beam mid-span, with 5, 15, and 22 mm depth. Figure 6 shows a study of the regression and performance of PSO-BOA-ANN in comparison with PSO-ANN, BOA-ANN, and GA-ANN with a hidden layer size  $n$  equal to 5. Table 4 provides a summary of the results.

The findings clearly demonstrate the superior performance of the hybrid PSO-BOA-ANN approach compared to individual methods such as PSO, BOA, and GA. The regression value obtained from the hybrid approach is close to 1, indicating a high level of accuracy. With a hidden layer size of  $n$  equal to 5, the maximum projected inaccuracy between the predicted and desired outcomes is estimated to be within the range of 0.02 mm. While PSO, BOA, and GA also exhibit the capability to forecast crack depths, the hybrid PSO-BOA approach outperforms them. This is primarily due to its wider error range and the fact that GA required more generations and populations, resulting in increased computational time. The detailed outcomes are presented in Fig. 7.

### 5.2 Damage case D<sub>2</sub>

By utilizing the identical crack depth values employed in the first scenario, we employed the PSO-BOA-ANN method to forecast the depths of the double cracks in the beam for this particular damage case. The regression performance of PSO-BOA-ANN was then compared to that of PSO-ANN, BOA-ANN, and GA-ANN, all with a hidden layer size of  $n$  equal to 5. Figure 8 illustrates this comparison. A comprehensive overview of the results can be found in Table 5.

Upon comparing the predicted and desired outcomes, it is observed that the maximum error for the PSO-BOA method falls within the range of 0.12 mm when the regression value approaches 1; however, the hybrid PSO-BOA requires fewer iterations. A study conducted by ANN enhanced with PSO-BOA found that ANN was more reliable than BOA and PSO separately in predicting crack depth in this damage case, while GA was less accurate and took longer to calculate. A list of the outcomes is shown in Fig. 9.

## 6 Experimental validation

In this experiment, aluminum specimens with the mechanical properties specified in Table 1 had their structural components triggered by an impact hammer, and the accelerometers estimated the results based on the acceleration properties. With the help of the DEWesoft data collecting system, beam specimens were studied. Figure 10 shows the device components and the experimental setup with the models of the damaged beam that are taken into

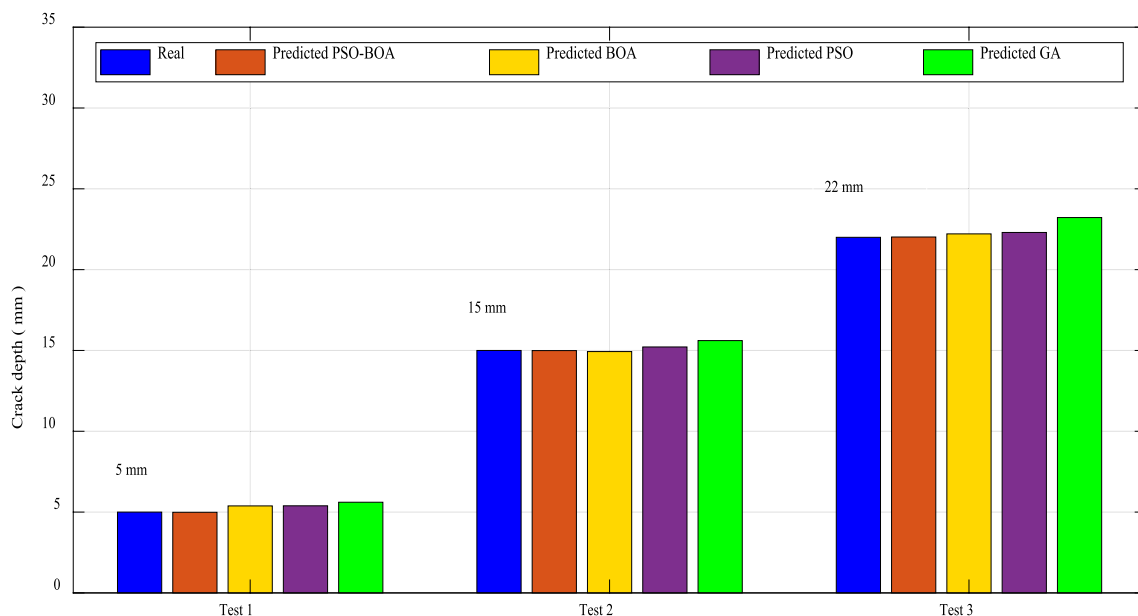


Fig. 7 Real and predicted cracks depths for damage case D<sub>1</sub>

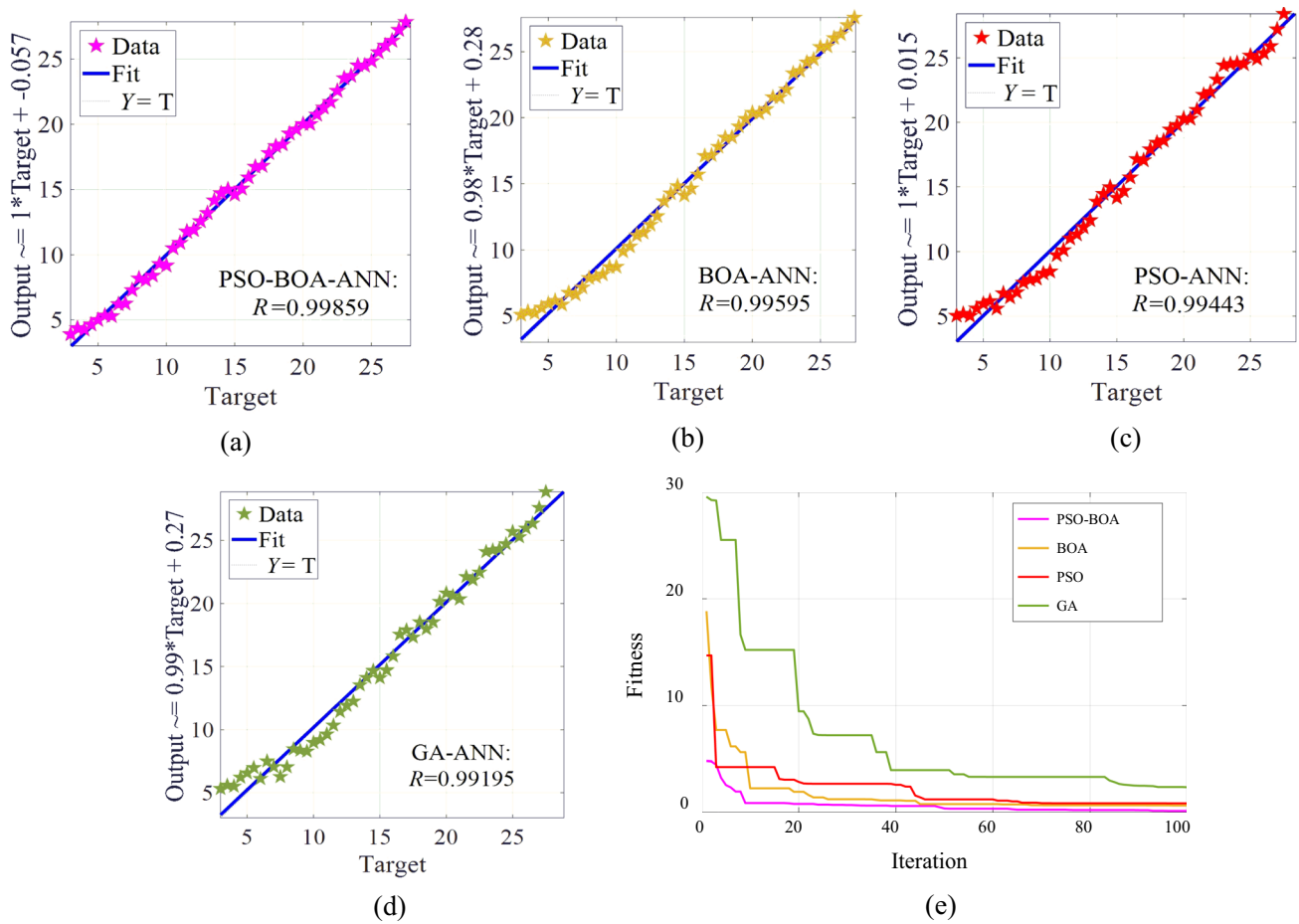


Fig. 8 Regression for damage case  $D_2$  with PSO-BOA (a), BOA (b), PSO (c), GA (d), and performance study (e)

Table 5 Crack depths predictions for damage case  $D_2$  using ANN trained by PSO-BOA, PSO, BOA, and GA

Damage case	Real crack depth (mm)	Predicted crack depth (mm)	Error in predicted results (%)	Fitness following number of iteration					
				1	25	50	75	100	
$D_2$	5	PSO-BOA	4.8888	2.224	4.71930	0.07199	0.00040	0.00040	0.00003
		BOA	4.8000	4.000	18.13683	2.32771	0.00701	0.00207	0.00075
		PSO	5.2091	4.182	15.25466	3.66211	0.01021	0.00388	0.00098
		GA	5.5354	10.708	30.02544	7.51254	4.02111	3.11209	2.10991
	15	PSO-BOA	14.9001	0.666	3.12132	0.00017	0.00017	0.00017	0.00017
		BOA	15.1311	0.874	3.10542	0.10522	0.00933	0.00135	0.00135
		PSO	15.1371	0.914	8.63585	0.88801	0.00502	0.00325	0.00091
		GA	15.6666	4.444	1.26544	1.00012	0.11564	0.02545	0.02545
	22	PSO-BOA	22.0099	0.045	0.51559	0.00204	0.00022	0.00022	0.00001
		BOA	22.2299	1.045	0.95712	0.12929	0.12929	0.03005	0.00457
		PSO	22.1999	0.909	1.99650	0.92658	0.12221	0.05252	0.00635
		GA	22.6999	3.181	1.65656	0.76520	0.32555	0.10010	0.08520

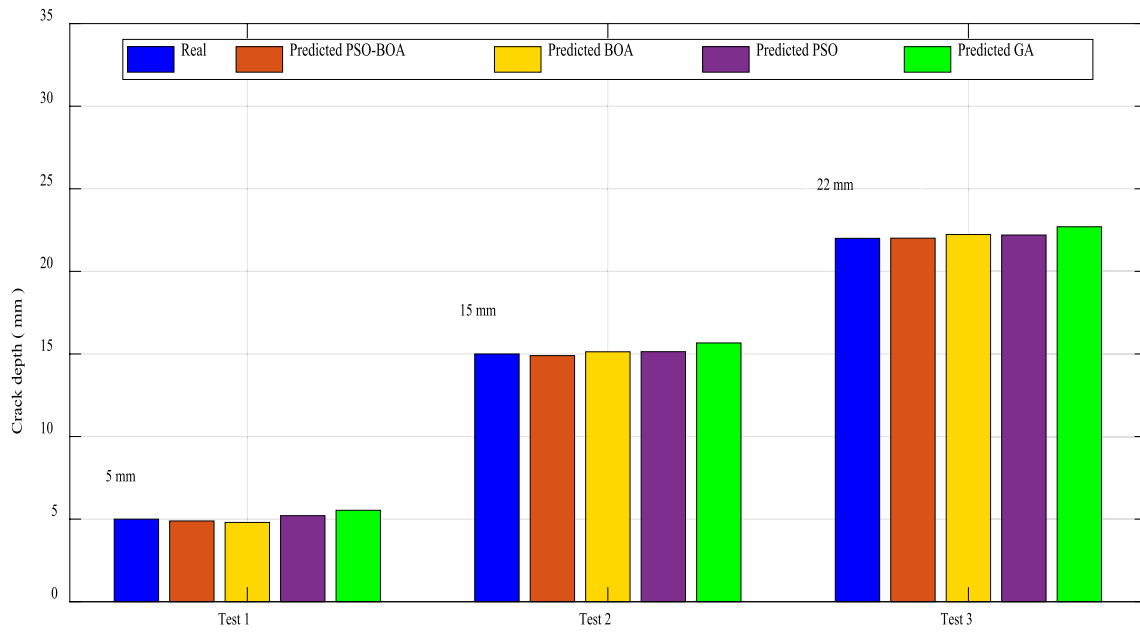


Fig. 9 Real and predicted cracks depths for damage case D<sub>2</sub>

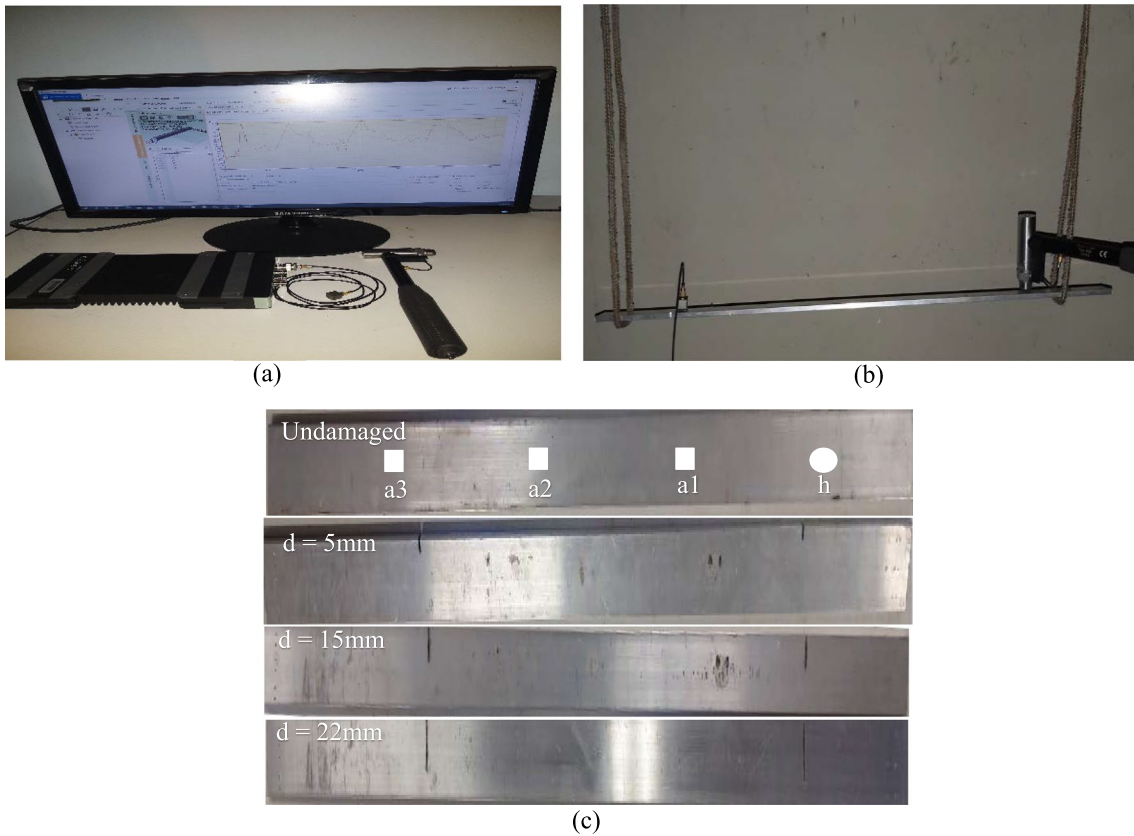


Fig. 10 Operating mode for cracked beam modal analysis. **a** Experimental device, **b** beam excitation mode, and **c** cracked beam models

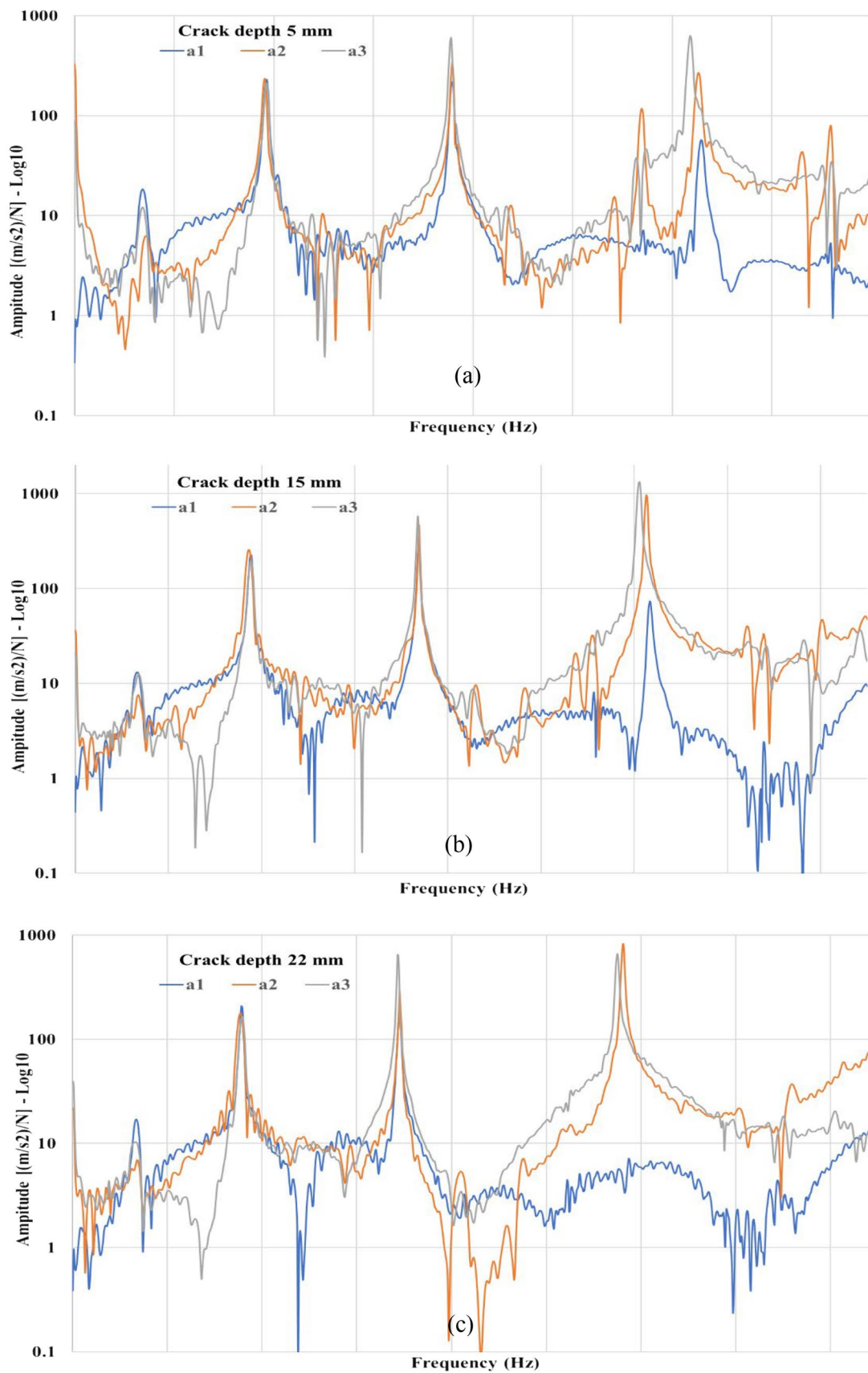
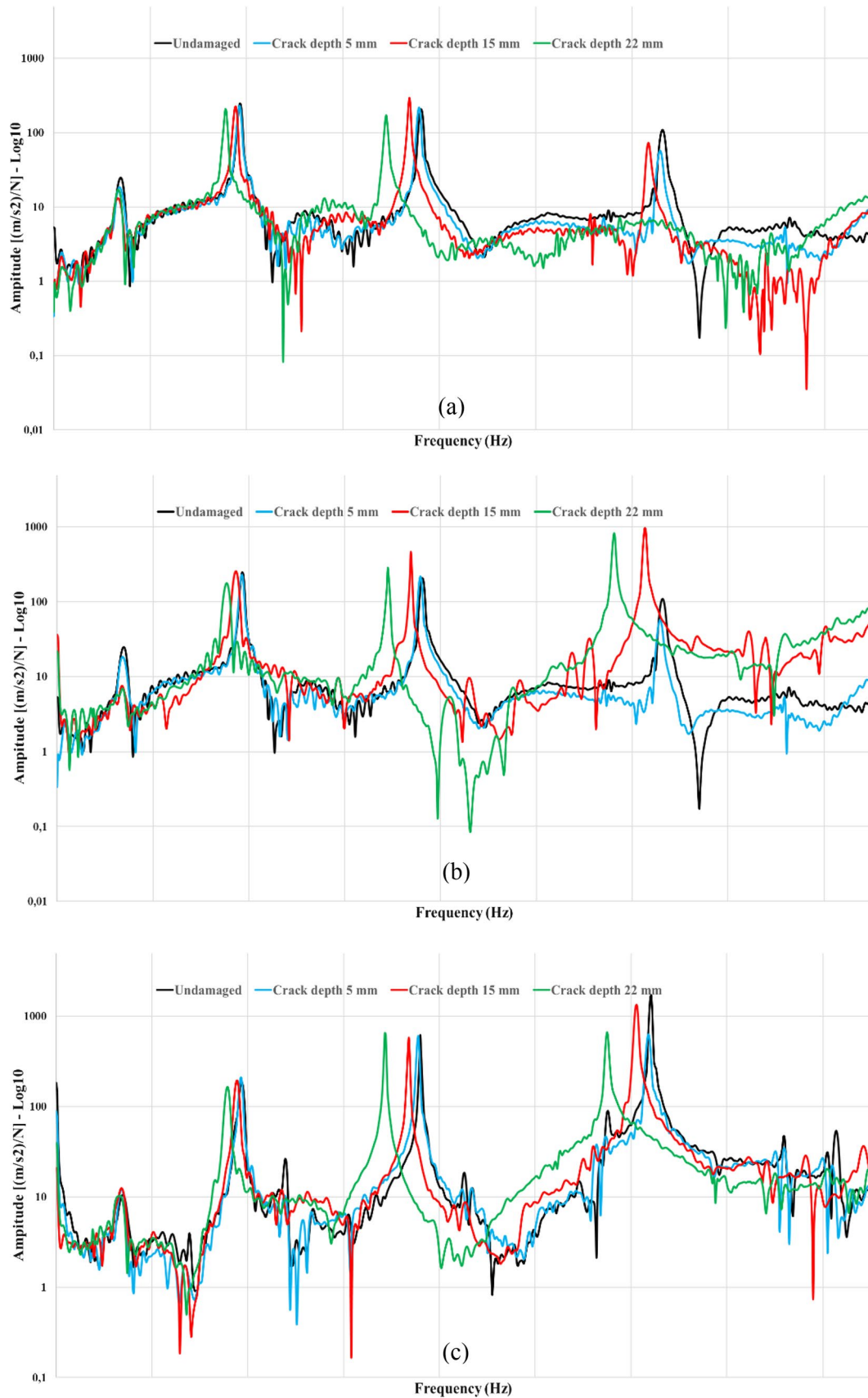


Fig. 11 Experimental envelope of FRF diagrams for damaged beam with crack depth 5 mm (a), 15 mm (b), and 22 mm (c) at accelerometer position  $a_1$ ,  $a_2$ , and  $a_3$



**Fig. 12** Comparison of envelopes of FRFs for undamaged and damaged with crack depth at accelerometer position  $a_1$  (a),  $a_2$  (b), and  $a_3$  (c)

**Table 6** Experimental and numerical frequency values for undamaged and damaged beam

Crack depth $d$ (mm)	Mode 1	Mode 2	Mode 3
0			
FEM	400.07	1085.1	2079.5
EXP	385.81	1097.65	2102.00
5			
FEM	396.33	1056.5	2013.4
EXP	383.22	1085.00	2055.25
15			
FEM	365.36	860.15	1601.8
EXP	370.78	1069.00	2048.11
22			
FEM	276.40	549.66	1118.2
EXP	287.00	888.00	1871.15

consideration. A Type 4508 piezoelectric accelerometer was installed at regular intervals of 200 mm on points labeled as a1, a2, and a3. To measure frequency values, a measurement device employing the Fast Fourier Transform (FFT) technique and Pulse software was utilized. For each accelerometer point (ai), a series of 10 hits (h) were generated, and the average value (h) for each hit was determined.

The experimental frequency response function (FRF) envelope, obtained from vibration measurements recorded by the accelerometer on beam models with double cracks, is shown in Figs. 11, 12. The cracks in the models have the same depth ( $d$ ) of 5, 15, and 22 mm, which were also considered in the numerical analysis. Table 6 presents a comparison of the experimental frequency values obtained for the damaged beams with their corresponding numerical values. To mitigate distortions and artifacts caused by aliasing and leakage phenomena, anti-aliasing filters are applied and windowing techniques are employed during frequency analysis. This helps address the issues and ensure accurate results without the negative effects of aliasing and leakage. The coherence in the experimental data was evaluated to assess the correlation and consistency between input and output signals, ensuring the reliability and validity of the measurements.

FRFs were acquired without explicitly accounting for damping effects. The focus of our study was on assessing the predictive capabilities of the hybrid PSO-BOA-ANN model for structural damage detection. The conversion from resonant frequency to natural frequency was achieved by taking into account the inherent characteristics of the beam specimens and employing established methodologies. This process allowed for an accurate estimation of the natural

frequency based on the measured resonant frequencies, ensuring consistency and reliability in the analysis. While damping effects were not explicitly incorporated, it is important to note that the experimental measurements were conducted under controlled conditions with minimal damping present.

This section data are used in order to test PSO-BOA-ANN's accuracy. Based on the experimental frequencies dataset in Table 6, the crack depth prediction model is tested using the parameters in Table 3. Figure 13 compares PSO-BOA-ANN regressions and convergences to PSO, BOA, and GA combined with ANN. Table 7 provides a summary of the results.

The maximum error range in crack depth prediction, when compared to PSO, BOA, and GA individually, is found to be within the range of 0.09 mm. In contrast, these algorithms exhibit a wider error range of up to 0.59 mm, requiring a significant number of generations and populations, and consuming more computational time. One physical reason behind the superior performance of PSO-BOA-ANN is its regression value, which is remarkably close to 1 when comparing the predicted and desired results. The utilization of ANN in conjunction with PSO-BOA yields the most accurate crack depth prediction for this particular damage case. Figure 14 provides a visual representation of the obtained outcomes.

## 7 Conclusion

In this study, a hybrid optimization algorithm is employed to detect cracks in a free-free aluminum beam. The algorithm combines PSO with BOA to improve both accuracy and convergence speed. To improve its training performance for damage prediction, the new hybrid algorithm PSO-BOA has been combined with ANN. Input data consist of natural frequencies obtained from numerical and experimental modal analysis, while output data consist of crack depths. The new approach was tested against existing methods of PSO-ANN, BOA-ANN, and GA-ANN to illustrate its accuracy.

The results show that PSO-BOA-ANN is the most successful hybrid algorithm for predicting crack depth out of all those that have been presented. However, PSO-BOA-ANN was slightly faster than PSO-ANN in its convergence, while BOA-ANN was the best with respect to computational time. This hybrid algorithm could be used for more complex structures.

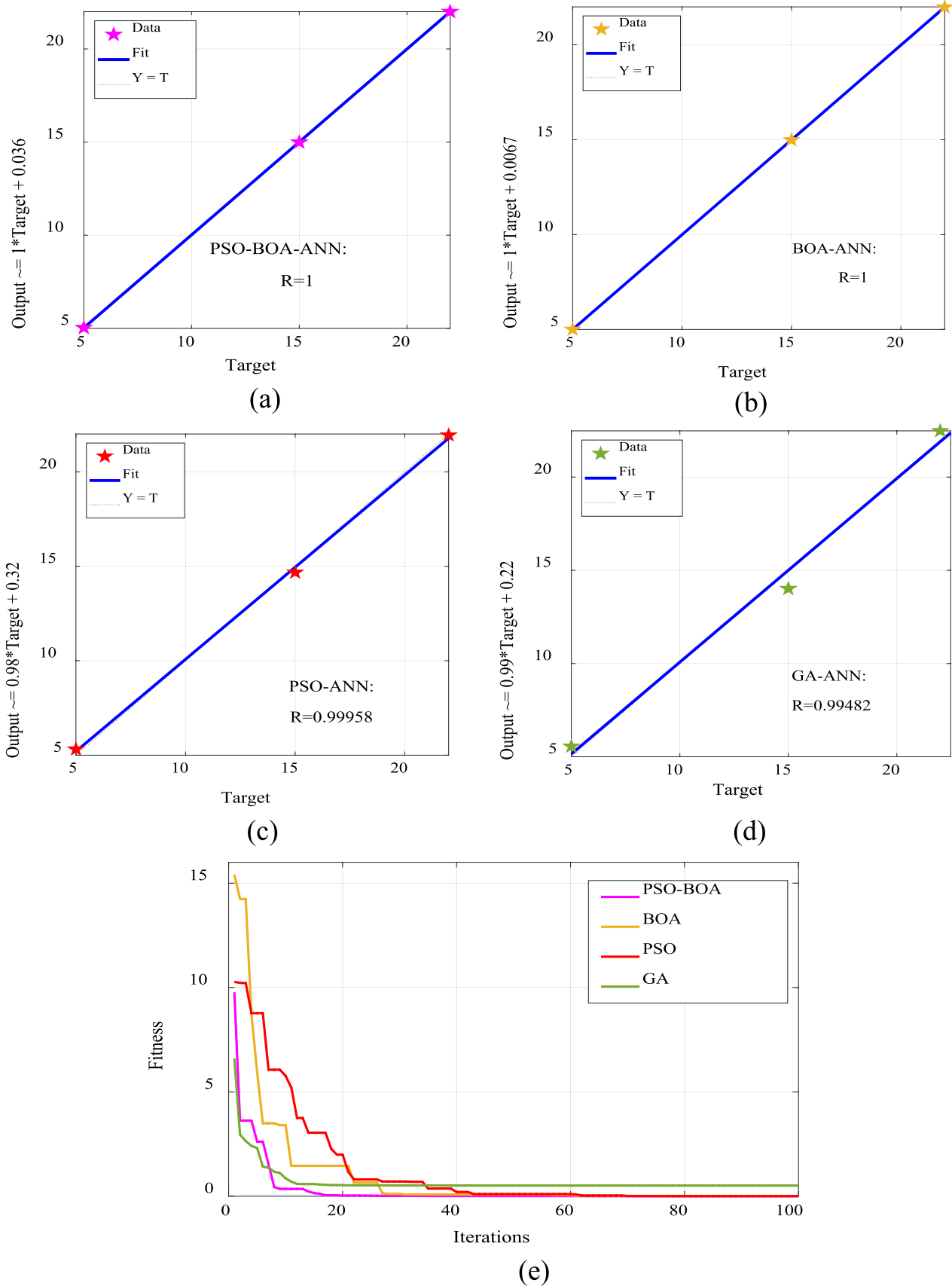
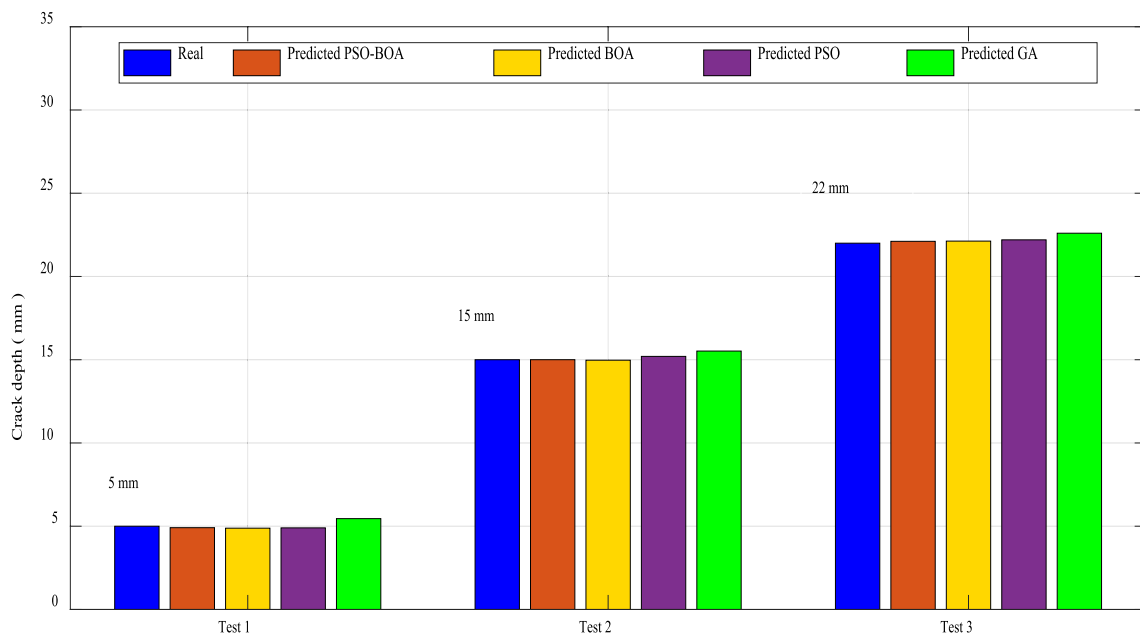


Fig. 13 Regression for ANN trained with PSO-BOA (a), BOA (b), PSO (c), GA (d), and performance study (e) for damaged beam with  $d = 15$  mm



**Table 7** Predicted double crack depth using experiment data and ANN trained by -PSO-BOA, BOA, PSO, and GA

Real experimental crack depth (mm)	Predicted crack depth (mm)	Error in predicted results (%)	Fitness following number of iteration					
			1	25	50	75	100	
5	PSO-BOA	4.9111	1.778	12.56354	0.00819	0.00333	0.00011	0.00011
	BOA	4.8822	2.356	10.46765	1.88808	0.21099	0.00229	0.00121
	PSO	4.8999	2.002	6.66772	2.22005	0.91125	0.00542	0.00091
	GA	5.4545	9.090	16.11222	4.10948	1.00212	0.89334	0.89334
15	PSO-BOA	15.0011	0.007	9.85104	0.00811	0.00009	0.00009	0.00002
	BOA	14.9711	0.192	15.42331	1.30343	0.05056	0.00211	0.00046
	PSO	15.1999	1.332	10.23435	1.62211	0.08092	0.00321	0.00067
	GA	15.5200	3.466	6.53233	1.23453	1.02222	1.02222	1.02222
22	PSO-BOA	22.1111	0.505	6.00293	0.18256	0.04445	0.00019	0.00019
	BOA	22.1246	0.566	2.99981	0.14445	0.00846	0.00846	0.00067
	PSO	22.1998	0.908	7.05864	0.92384	0.00888	0.00888	0.00111
	GA	22.5985	2.720	7.24858	1.88888	0.92434	0.09001	0.01012



**Fig. 14** Crack prediction using ANN trained by PSO-BOA, BOA, PSO, and GA for experimental data

While our results demonstrated the effectiveness and accuracy of the proposed method under controlled experimental conditions, it is important to acknowledge its limitations and areas for future improvement. One limitation of our study is the assumption of noise-free conditions, which may not reflect real-service environments. Future work should focus on incorporating noise effects and developing robust techniques to separate external factors from actual damage signals. Additionally, the current

study mainly focused on crack depth prediction and did not explore other types of damage. Future research can expand the application of the hybrid approach to various damage types and investigate its performance in more complex structural systems. Overall, addressing these limitations and considering noise effects will contribute to enhancing the practical applicability and reliability of the proposed method in real-world structural health monitoring applications.

## Appendix

Frequency values of different cracks depth in both damaged scenarios.

Crack depth (mm)	Single crack			Double crack		
	Mode 1 (Hz)	Mode 2 (Hz)	Mode 3 (Hz)	Mode 1 (Hz)	Mode 2 (Hz)	Mode 3 (Hz)
0.5	399.68	1084.4	2077.2	399.47	1082.1	2072.1
1	399.35	1084.4	2076.0	399.34	1081.0	2069.7
1.5	398.87	1084.4	2074.2	399.15	1079.5	2066.1
2	398.26	1084.4	2071.9	398.91	1077.5	2061.4
2.5	397.50	1084.4	2069.1	398.62	1075.0	2055.8
3	396.62	1084.4	2065.7	398.27	1072.2	2049.2
3.5	395.59	1084.4	2061.7	397.87	1068.9	2041.6
4	394.44	1084.4	2057.4	397.41	1065.2	2033.1
4.5	393.16	1084.4	2052.7	396.90	1061.1	2023.7
5	391.75	1084.4	2047.6	396.33	1056.5	2013.4
5.5	390.20	1084.4	2041.9	395.71	1051.5	2002.2
6	388.52	1084.4	2035.9	395.02	1046.2	1990.0
6.5	386.69	1084.4	2029.4	394.26	1040.3	1976.9
7	384.72	1084.3	2022.4	393.44	1034.0	1962.9
7.5	382.59	1084.3	2014.9	392.54	1027.3	1947.9
8	380.31	1084.3	2007.0	391.57	1020.1	1932.0
8.5	377.87	1084.3	1998.7	390.52	1012.4	1915.1
9	375.26	1084.2	1989.8	389.37	1004.2	1897.2
9.5	372.47	1084.2	1980.5	388.13	995.47	1878.3
10	369.50	1084.1	1970.7	386.79	986.22	1858.4
10.5	366.33	1084.1	1960.4	385.34	976.42	1837.4
11	362.97	1084.0	1949.6	383.77	966.05	1815.5
11.5	359.39	1084.0	1938.3	382.07	955.10	1792.4
12	356.03	1083.9	1926.5	380.23	943.53	1768.4
12.5	355.60	1083.9	1914.2	378.23	931.34	1743.2
13	355.15	1083.8	1901.3	376.06	918.49	1717.0
13.5	354.68	1083.7	1888.0	373.71	904.97	1689.8
14	354.18	1083.6	1874.2	371.16	890.76	1661.5
14.5	353.67	1083.5	1859.8	368.38	875.82	1632.1
15	353.13	1083.4	1845.0	365.36	860.15	1601.8
15.5	352.57	1083.3	1829.7	362.07	843.71	1570.5
16	351.99	1083.2	1813.9	358.48	826.49	1538.4
16.5	351.38	1083.1	1797.7	354.55	808.46	1505.3
17	350.74	1082.9	1781.0	350.26	789.60	1471.6
17.5	350.07	1082.8	1764.0	345.56	769.87	1437.0
18	349.37	1082.6	1746.6	340.41	749.28	1401.9
18.5	348.64	1082.5	1728.9	334.76	727.78	1366.4
19	347.88	1082.3	1710.9	328.56	705.35	1330.5
19.5	347.08	1082.1	1692.7	321.75	681.96	1294.4
20	346.24	1081.9	1674.3	314.28	657.59	1258.4
20.5	345.35	1081.7	1655.8	306.07	632.21	1222.5
21	344.42	1081.4	1637.3	297.07	605.78	1187.0
21.5	343.44	1081.2	1618.8	287.20	578.27	1152.2

Crack depth (mm)	Single crack			Double crack		
	Mode 1 (Hz)	Mode 2 (Hz)	Mode 3 (Hz)	Mode 1 (Hz)	Mode 2 (Hz)	Mode 3 (Hz)
22	342.40	1080.9	1600.4	276.40	549.66	1118.2
22.5	341.29	1080.6	1582.2	264.62	519.92	1085.3
23	340.11	1080.2	1564.2	251.81	489.02	1053.8
23.5	338.85	1079.8	1546.5	237.92	456.96	1023.7
24	337.49	1079.4	1529.1	222.95	423.75	995.47
24.5	336.02	1078.9	1512.3	206.89	389.41	969.14
25	334.42	1078.3	1495.9	189.78	354.00	944.88

**Funding** Open access funding provided by Università Politecnica delle Marche within the CRUI-CARE Agreement.

**Data availability** The data that support the findings of this study are available from the corresponding author upon reasonable request.

## Declarations

**Conflict of interest** The authors declare that they have no known competing financial interests or personal relationships that could have appeared to influence the work reported in this paper.

**Open Access** This article is licensed under a Creative Commons Attribution 4.0 International License, which permits use, sharing, adaptation, distribution and reproduction in any medium or format, as long as you give appropriate credit to the original author(s) and the source, provide a link to the Creative Commons licence, and indicate if changes were made. The images or other third party material in this article are included in the article's Creative Commons licence, unless indicated otherwise in a credit line to the material. If material is not included in the article's Creative Commons licence and your intended use is not permitted by statutory regulation or exceeds the permitted use, you will need to obtain permission directly from the copyright holder. To view a copy of this licence, visit <http://creativecommons.org/licenses/by/4.0/>.

## References

- Bao Y, Chen Z, Wei S, Xu Y, Tang Z, Li H (2019) The state of the art of data science and engineering in structural health monitoring. *Engineering* 5(2):234–242. <https://doi.org/10.1016/j.eng.2018.11.027>
- Silva RN, Tsuruta KM, Rabelo DS, Finzi Neto RM, Cavallini AA, Steffen V (2020) Impedance-based structural health monitoring applied to steel fiber-reinforced concrete structures. *J Braz Soc Mech Sci Eng* 42(7):1–15. <https://doi.org/10.1007/s40430-020-02458-4>
- Anas M, Nasir MA, Asfar Z, Nauman S, Akalin M, Ahmad F (2018) Structural health monitoring of GFRP laminates using graphene-based smart strain gauges. *J Braz Soc Mech Sci Eng* 40(8):1–10. <https://doi.org/10.1007/s40430-018-1320-4>
- He XH, Hua XG, Chen ZQ, Huang FL (2011) EMD-based random decrement technique for modal parameter identification of an existing railway bridge. *Eng Struct* 33(4):1348–1356. <https://doi.org/10.1016/j.engstruct.2011.01.012>
- Wang H, Tao T, Li A, Zhang Y (2016) Structural health monitoring system for Sutong cable-stayed bridge. *Smart Struct Syst* 18(2):317–334. <https://doi.org/10.12989/sss.2016.18.2.317>

6. Cigada A, Moschioni G, Vanali M, Caprioli A (2010) The measurement network of the San Siro Meazza Stadium in Milan: origin and implementation of a new data acquisition strategy for structural health monitoring. *Exp Tech* 34(1):70. <https://doi.org/10.1111/j.1747-1567.2009.00536.x>
7. Zhou GD, Yi TH (2013) Recent developments on wireless sensor networks technology for bridge health monitoring. *Math Probl Eng*. <https://doi.org/10.1155/2013/947867>
8. Mistry K, Zhang L, Neoh SC, Lim CP, Fielding B (2016) A micro-GA embedded PSO feature selection approach to intelligent facial emotion recognition. *IEEE Trans Cybern* 47(6):1496–1509. <https://doi.org/10.1109/TCYB.2016.2549639>
9. Fathnejat H, Ahmadi-Nedushan B (2020) An efficient two-stage approach for structural damage detection using meta-heuristic algorithms and group method of data handling surrogate model. *Front Struct Civ Eng* 14(4):907–929. <https://doi.org/10.1007/s11709-020-0628-1>
10. Hamdia KM, Zhuang X, Rabczuk T (2021) An efficient optimization approach for designing machine learning models based on genetic algorithm. *Neural Comput Appl* 33(6):1923–1933. <https://doi.org/10.1007/s00521-020-05035-x>
11. Mohan SC, Maiti DK, Maity D (2013) Structural damage assessment using FRF employing particle swarm optimization. *Appl Math Comput* 219(20):10387–10400. <https://doi.org/10.1016/j.amc.2013.04.016>
12. Shamshirband S, Mosavi A, Rabczuk T (2020) Particle swarm optimization model to predict scour depth around a bridge pier. *Front Struct Civ Eng* 14(4):855–866. <https://doi.org/10.1007/s11709-020-0619-2>
13. Ghodsi H, Khanjani MJ, Beheshti AA (2018) Evaluation of harmony search optimization to predict local scour depth around complex bridge piers. *Civil Engineering Journal* 4(2):402–412
14. Mottahedi A, Sereshki F, Ataei M (2018) Overbreak prediction in underground excavations using hybrid ANFIS-PSO model. *Tunn Undergr Space Technol* 80:1–9. <https://doi.org/10.1016/j.tust.2018.05.023>
15. Bassar H, Karami H, Shamshirband S, Akib S, Amirmojahedi M, Ahmad R, Javidnia H (2015) Hybrid ANFIS–PSO approach for predicting optimum parameters of a protective spur dike. *Appl Soft Comput* 30:642–649. <https://doi.org/10.1016/j.asoc.2015.02.011>
16. Gandomi AH, Yang XS, Alavi AH (2013) Cuckoo search algorithm: a metaheuristic approach to solve structural optimization problems. *Eng Comput* 29(1):17–35. <https://doi.org/10.1007/s00366-011-0241-y>
17. Xu HJ, Liu JK, Lu ZR (2016) Structural damage identification based on cuckoo search algorithm. *Adv Struct Eng* 19(5):849–859. <https://doi.org/10.1177/1369433216630128>
18. Khatir A, Tehami M, Khatir S, Abdel Wahab M (2016) Multiple damage detection and localization in beam-like and complex structures using co-ordinate modal assurance criterion combined with firefly and genetic algorithms. *J Vibroeng* 18(8):5063–5073. <https://doi.org/10.21595/jve.2016.17026>
19. Sun H, Luş H, Betti R (2013) Identification of structural models using a modified Artificial Bee Colony algorithm. *Comput Struct* 116:59–74. <https://doi.org/10.1016/j.compstruc.2012.10.017>
20. Yu L, Xu P (2011) Structural health monitoring based on continuous ACO method. *Microelectron Reliab* 51(2):270–278. <https://doi.org/10.1016/j.microrel.2010.09.011>
21. Khatir A, Tehami M, Khatir S, Wahab MA (2016) Damage detection and localization on thin plates using vibration analysis. *Res Vet Sci* 106:107–111
22. Tsai PW, Pan JS, Liao BY, Tsai MJ, Istanda V (2012) Bat algorithm inspired algorithm for solving numerical optimization problems. *Appl Mech Mater* 148:134–137. <https://doi.org/10.4028/www.scientific.net/AMM.148-149.134>
23. Miguel LFF, Miguel LFF, Kaminski J Jr, Riera JD (2012) Damage detection under ambient vibration by harmony search algorithm. *Expert Syst Appl* 39(10):9704–9714. <https://doi.org/10.1016/j.eswa.2012.02.147>
24. Gomes GF, de Almeida FA, Junqueira DM, da Cunha Jr SS, Ancelotti AC Jr (2019) Optimized damage identification in CFRP plates by reduced mode shapes and GA-ANN methods. *Eng Struct* 181:111–123. <https://doi.org/10.1016/j.engstruct.2018.11.081>
25. Na C, Kim SP, Kwak HG (2011) Structural damage evaluation using genetic algorithm. *J Sound Vib* 330(12):2772–2783. <https://doi.org/10.1016/j.jsv.2011.01.007>
26. Yildiz AR (2013) Cuckoo search algorithm for the selection of optimal machining parameters in milling operations. *Int J Adv Manuf Technol* 64(1):55–61. <https://doi.org/10.1007/s00170-012-4013-7>
27. Jung DS, Kim CY (2013) Finite element model updating on small-scale bridge model using the hybrid genetic algorithm. *Struct Infrastruct Eng* 9(5):481–495. <https://doi.org/10.1080/15732479.2011.564635>
28. Kellouche Y, Ghrici M, Boukhatem B (2021) Service life prediction of fly ash concrete using an artificial neural network. *Front Struct Civ Eng* 15(3):793–805. <https://doi.org/10.1007/s11709-021-0717-9>
29. Liu F, Ding W, Qiao Y, Wang L (2020) An artificial neural network model on tensile behavior of hybrid steel-PVA fiber reinforced concrete containing fly ash and slag powder. *Front Struct Civ Eng* 14(6):1299–1315. <https://doi.org/10.1007/s11709-020-0712-6>
30. Hamdia KM, Lahmer T, Nguyen-Thoi T, Rabczuk T (2015) Predicting the fracture toughness of PNCs: a stochastic approach based on ANN and ANFIS. *Comput Mater Sci* 102:304–313. <https://doi.org/10.1016/j.commatsci.2015.02.045>
31. Khatir A, Capozucca R, Khatir S, Magagnini E (2022) Vibration-based crack prediction on a beam model using hybrid butterfly optimization algorithm with artificial neural network. *Front Struct Civ Eng*. <https://doi.org/10.1007/s11709-022-0840-2>
32. Khatir A, Capozucca R, Khatir S, Magagnini E, Benaissa B, Le Thanh C, Wahab MA (2023) A new hybrid PSO-YUKI for double cracks identification in CFRP cantilever beam. *Compos Struct* 311:116803. <https://doi.org/10.1016/j.compstruct.2023.116803>
33. Khatir A, Capozucca R, Magagnini E, Khatir S, Bettucci E (2022) Structural health monitoring for RC beam based on RBF neural network using experimental modal analysis. In: international conference of steel and composite for engineering structures (pp. 82–92). Cham: Springer International Publishing. [https://doi.org/10.1007/978-3-031-24041-6\\_7](https://doi.org/10.1007/978-3-031-24041-6_7)
34. Dunant CF, Bordas S, Kerfriden P, Scrivener KL, Rabczuk T (2011) An algorithm to compute damage from load in composites. *Front Arch Civ Eng China* 5(2):180–193. <https://doi.org/10.1007/s11709-011-0107-9>
35. Jierula A, Oh TM, Wang S, Lee JH, Kim H, Lee JW (2021) Detection of damage locations and damage steps in pile foundations using acoustic emissions with deep learning technology. *Front Struct Civ Eng* 15(2):318–332
36. Gelman L (2010) The new frequency response functions for structural health monitoring. *Eng Struct* 32(12):3994–3999. <https://doi.org/10.1016/j.engstruct.2010.09.010>
37. Wang XJ, Zhou XQ, Xia Y, Weng S (2013) Comparisons between modal-parameter-based and flexibility-based damage identification methods. *Adv Struct Eng* 16(9):1611–1619. <https://doi.org/10.1260/1369-4332.16.9.1611>

38. Capozucca R, Khatir A, Magagnini E (2022) Experiences on anchorage systems for FRP rods. In: International conference of steel and composite for engineering structures (pp. 48–58). Cham: Springer International Publishing. [https://doi.org/10.1007/978-3-031-24041-6\\_4](https://doi.org/10.1007/978-3-031-24041-6_4)
39. Nozarian MM, Esfandiari A (2009) Structural damage identification using frequency response function. *Mater Forum* 33:443–449
40. Capozucca R (2013) A reflection on the application of vibration tests for the assessment of cracking in PRC/RC beams. *Eng Struct* 48:508–518. <https://doi.org/10.1016/j.engstruct.2012.09.022>
41. Capozucca R, Bonci B (2015) Notched CFRP laminates under vibration. *Compos Struct* 122:367–375. <https://doi.org/10.1016/j.compstruct.2014.11.062>
42. Salehi M, Ziaei-rad S, Ghayour M, Vazirizanjani MA (2010) A structural damage detection technique based on measured frequency response functions. *Contempor Eng Sci* 3(5):215–226
43. Golafshani AA, Kianian M, Ghodrati E (2010) Health monitoring of structures using few frequency response measurements. *Sci Iran* 17(6):493–500
44. Zhang M, Long D, Qin T, Yang J (2020) A chaotic hybrid butterfly optimization algorithm with particle swarm optimization for high-dimensional optimization problems. *Symmetry* 12(11):1800. <https://doi.org/10.3390/sym12111800>
45. Arora S, Singh S (2019) Butterfly optimization algorithm: a novel approach for global optimization. *Soft Comput* 23:715–734. <https://doi.org/10.1007/s00500-018-3102-4>

**Publisher's Note** Springer Nature remains neutral with regard to jurisdictional claims in published maps and institutional affiliations.